EUMETSAT OSI SAF
OCEAN AND SEA ICE

# Scientific Validation Report for the Geostationary Satellite Sea Surface Temperature

## Meteosat SST: OSI-206-a

## GOES-East SST: OSI-207-b

## Meteosat Indian Ocean SST: OSI-IO-SST

Version: 3.0
Date: 01/10/2023

N. Nano-Ascione, S. Saux Picart

METEO FRANCE

# Documentation change record

| Version | Date | Authors | Description |
|---|---|---|---|
| **0.1** | 06/11/2019 | MF/CMS | Initial submitted version |
| **1.0** | 19/02/2020 | MF/CMS | Revised version for ORR: added table of monthly statistics in section 3.2. |
| **2.0** | 01/12/2022 | MF/CMS | Revised version : validation for Meteosat-9 OSI-IO-SST and recent statistics for GOES-16 and Meteosat-11. |
| **3.0** | 01/10/2023 | MF/CMS | Revised version : validation for Meteosat-10 OSI-206-a : swap Meteosat-11 to Meteosat-10 on 0° position on the 21th March 2023. |

# Contents

# List of Figures



# List of Tables

# 1 Introduction

The EUMETSAT Satellite Application Facilities (SAFs) are dedicated centres of excellence for processing satellite data. They form an integral part of the distributed EUMETSAT Application Ground Segment. The Ocean and Sea Ice SAF, led by Météo-France/Centre de Météorologie Spatiale (MF/CMS), has the responsibility of developing, validating and distributing near real time products of Sea Surface Temperature (SST), radiative fluxes, wind and Sea Ice for a variety of platforms/sensors.

In this context OSI SAF is processing Sea Surface Temperature products from geostationary satellite from the EUMETSAT Meteosat Second Generation program and the US program of NASA and the National Oceanic and Atmospheric Administration (NOAA), Geostationary Operational Environment Satellite (GOES) in East position.

More specifically OSI SAF is providing the user community with the products presented in table 1.

*Table 1: Current geostationary SST products summary.*

| Product ID | Satellite / instrument | Spatial coverage | Spatial sampling | Frequency | Reference |
|---|---|---|---|---|---|
| **OSI-206-a** | Meteosat-10 / SEVIRI | 60°N to 60°S<br>60°W – 60°E | 0.05°<br>Lat-Lon | hourly | [AD.1] |
| **OSI-207-b** | GOES-16 / ABI | 60°N to 60°S<br>135°W – 15°W | 0.05°<br>Lat-Lon | hourly | [AD.1] |
| **OSI-IO-SST** | Meteosat-9 / SEVIRI | 60°N to 60°S<br>19.5°W – 101.5°E | 0.05°<br>Lat-Lon | hourly | |

## 1.1 Purpose and scope of the document

This document is the scientific validation report for the OSI SAF geostationary SST products. It

*Table 2: Threshold, target and optimal accuracies define respectively: the lower limit of usefulness, the main reference for assessment at EUMETSAT and the optimal performance reachable in theory provided the instrument characteristics. Extracted from [AD.1].*

| Product ID | Threshold accuracy. Monthly bias, SD | Target accuracy. Monthly bias, SD | Optimal accuracy. Monthly bias, SD |
|---|---|---|---|
| **OSI-206-a**<br>**OSI-207-b** | 1K, 1.5K | 0.5K, 1.0K | 0.1K, 0.5K |
| **OSI-IO-SST** | The above values are considered | | |

The intention of this report is to evaluate the quality of the OSI SAF geostationary products and their compliance with the product requirement of the third Continuous Development and Operation Phase (CDOP-3) which are summarised in table 2.

This document is complemented by the Algorithm Theoretical Basis Document for Geostationary Satellite Sea Surface Temperature [RD.1] and the Geostationary Sea Surface Temperature Product User Manual [RD.2].

## 1.2 Reference documents

| Ref | Title | Code |
|---|---|---|
| [RD.1] | Algorithm Theoretical Basis Document for Geostationary Satellite Sea Surface Temperature version 1.2 | SAF/OSI/CDOP3/SCI/MA/342 |
| [RD.2] | Geostationary Sea Surface Temperature Product User Manual OSI-206-a, OSI-207-b, OSI-IO-SST | SAF/OSI/MF/TEC/MA/181 |

## 1.3 Applicable documents

| Ref | Title | Code |
|---|---|---|
| **[AD.1]** | OSI SAF CDOP 4, Product Requirement Document version 1.0 | SAF/OSI/CDOP4/MF/MGT/PL/4-001 |
| **[AD.2]** | OSI SAF Service Specification version 2.0 | SAF/OSI/CDOP4/MF/MGT/PL/003 |

## 1.4 Acronyms

| | |
|---|---|
| AVHRR | Advanced Very High Resolution Radiometer |
| BT | Brightness Temperature |
| CDOP | Continuous Development and Operation Phase |
| GOES | Geostationary Operational Environment Satellite |
| GTS | Global Telecommunication System |
| IR | Infra-Red |
| MF/CMS | Météo-France/Centre de Météorologie Spatiale |
| MDS | Match-up Data Set |
| NOAA | National Oceanic and Atmospheric Administration |
| NWP | Numerical Weather Prediction |
| OSI SAF | Ocean and Sea Ice Satellite Application Facility |
| OSTIA | Operational Sea Surface Temperature and Sea Ice Analysis |
| QL | Quality Level |
| RTTOV | Radiative Transfer for TOVS |
| SAF | Satellite Application Facility |
| SDI | Saharan Dust Index |
| SEVIRI | Spinning Enhanced Visible and InfraRed Imager |
| SSES | Sensor Specific Error Statistics |
| SST | Sea Surface Temperature |
| SD | Standard Deviation |
| TIROS | Television Infrared Observation Satellite |
| TOVS | TIROS Operational Vertical Sounder |

# 2 Overview of SST retrieval

In this section a brief overview of processing of SST for geostationary satellite and the creation of match-up data set used in this report for validation. All the details are given in [RD.1].

## 2.1 Sea surface temperature computation

SST is computed for all clear-sky water pixels. Clear-sky pixels are identified using an external cloud mask as input to the processing. A cloud mask control procedure is used to assign a lower quality level to pixels which are dubious (thin cloud, dust aerosols,...). It consists of a series of tests that consider various quantities such as the local values of the gradient, temperature, probability of ice, etc. The quality level is provided at the pixel level with increasing reliability from 2 (="bad") to 5 (="excellent"); 0 means unprocessed and 1 means cloudy. Quality levels give the user a simple means of filtering the data. Users are advised to use quality levels 3 to 5 for quantitative applications. These quality levels are used in the analysis presented in the following sections, and only results of validation for quality levels 3 to 5 are shown.

For all geostationary satellite, the computation of SST is based on a quasi-linear algorithm using brightness temperatures such as the ones presented in McCain et al. (1985); Walton et al. (1998). The generic form of the algorithm is:

$$\hat{x} = a_0 + \mathbf{a}^\top \mathbf{y}_0 \tag{1}$$

where, $\hat{x}$ is the estimated SST, $a_0$ is an offset coefficient, $\mathbf{a}$ is a column vector of weighting coefficients and $\mathbf{y}_0$ contains the observed BTs. The coefficients contained in the vector $\mathbf{a}$ are functions of SST climatology and satellite zenith angle.

This type of algorithm, when used for global applications, induces regional and seasonal biases (e.g. Marsouin et al. (2015)). In order to correct for these, an algorithm correction method is used (Le Borgne et al., 2011). It relies on brightness temperature simulations from the RTTOV radiative transfer model using NWP atmospheric profiles and OSTIA SSTs (Donlon et al., 2012). Simulations are performed for each clear sky pixel identified as such with the cloud mask. Simulations are not perfect, due to model output errors, RTTOV errors and instrument calibration errors. They are therefore adjusted using an empirical approach based on averaging the simulated minus observed BT differences over 3 days centred on the day being processed. The correction is calculated as the difference between the retrieved SST from simulated adjusted BTs and the SST analysis used as input to the simulations.

## 2.2 Geostationary SST products

OSI SAF process data from three geostationary satellites: currently GOES-16 (in East position), Meteosat-9 on the Indian Ocean and Meteosat-10 over the Atlantic Ocean. The field of view of the three satellites are illustrated on Figure 1. Data are processed at full spatial resolution and aggregated as hourly product on a regular lat/lon grid.

Details about the products can be found in the Product User Manual [RD.2].

## 2.3 The match-up data set (MDS)

All validation procedures require a MDS has been elaborated. In an operational prospective, the MDS gathers in situ SST measurements from ship, moored buoys and drifting buoys available through the Global Telecommunication System (GTS). Collocated full resolution satellite information is added in a 3 hours time frame around the measurement. It consists in all the variables included in the intermediate workfile extracted in a box around the in situ measurements. The MDS for day $d$ is currently elaborated with a five days delay ($d$+5) to ensure nearly all in situ data are available through GTS. For the purpose of operational validation:

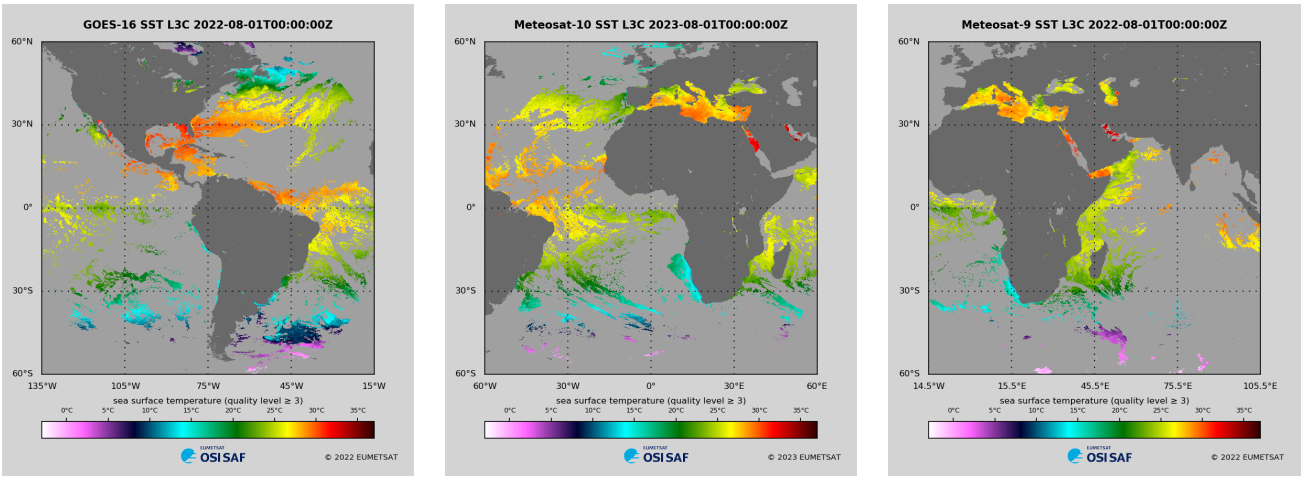


*Figure 1: SST from GOES-16 (left), Meteosat-10 (center), and Meteosat-9 (right).*

- Only drifting buoys are considered.
- Only the central SST of each box is used.
- Night-time and day-time algorithm are validated separately.
- The time difference between satellite SST and in situ measurement should not exceed 30 minutes.

Additional tests are designed to filter out dubious in situ measurements:

- A blacklist of dubious buoys is kept up-to-date at Météo-France. This blacklist is applied before validation.
- SST in situ measurement more than 5K different from climatological SST are eliminated.

All subsequent results are based on the exploitation of the MDS.

# 3 Assessment of OSI SAF geostationary SST products

## 3.1 Statistics of comparison

The SST retrieved is assessed in terms of its difference to in situ measurements from drifting buoys. Normal statistics (bias and standard deviation (SD) of the difference ($\Delta$SST = $SST_{sat} - SST_{in\,situ}$) are computed and presented as well as robust statistics (median and Robust Standard Deviation: RSD = [$75^{th}$ percentile of $\Delta$SST − $25^{th}$ percentile of $\Delta$SST]/1.348)

These statistics are usually computed on the whole disk of view for various time intervals (month, trimester or whole duration) and presented hereafter.

Only satellite SST quality level 3 to 5 are assessed unless otherwise stated. SSES biases have not been applied.

## 3.2 Overall statistics

In this section we present the results for the entire field of view of each satellite and a time period as follow:

- GOES-16 (OSI-207-a) : from 2021/11/1 to 2022/10/31
- Meteosat-10 (OSI-206-a) : from 2023/04/01 to 2023/08/31
- Meteosat-9 (OSI-IO-SST) : from 2022/07/01 to 2022/10/31

For GOES-16 the period of validation is one year, for Meteosat-10 it is 5 months since the switch of the satellite over 0° position and for Meteosat-9 it is 4 months since the switch of the satellite over Indian Ocean.

Table 3 shows the result of comparison to drifting buoy measurements for pixel quality level 3, 4 and 5 together. In general bias is better than 0.1K in absolute value and standard deviation is lower than 0.5K for GOES-16. The standard deviation for Meteosat-10 and Meteosat-9 is better than the target accuracy of 1.0K, it is around and a little higher than 0.5K which is the optimal accuracy. Slightly better statistics are obtained for GOES-16 with, in particular, a standard deviation of 0.39 during daytime. The reason explaining these better results is the use of a three channel algorithm (see [RD.1]).

*Table 3: Statistics of the difference between satellite SST and drifting buoy measurements computed: Mean (Bias), standard deviation (SD), median and Robust Standard Deviation (RSD). N is the number of match-ups.*

| | Night | | | | | Day | | | | |
|---|---|---|---|---|---|---|---|---|---|---|
| | N | Bias | SD | Med | RSD | N | Bias | SD | Med | RSD |
| GOES-16 (OSI-207-b) | 257981 | -0.01 | 0.42 | 0.02 | 0.35 | 248690 | 0.14 | 0.39 | 0.16 | 0.30 |
| Meteosat-10 (OSI-206-a) | 100172 | -0.18 | 0.50 | -0.16 | 0.44 | 160778 | -0.13 | 0.53 | -0.09 | 0.42 |
| Meteosat-9 (OSI-IO-SST) | 25743 | -0.02 | 0.55 | -0.01 | 0.44 | 40142 | 0.06 | 0.56 | 0.06 | 0.45 |

Tables 4, 5 and 6 contain similar statistics as table 3 split by quality level. One can notice the clear improvement of the statistics as the quality level goes up. Readers' attention is drawn to the degraded statistics for quality level pixels equal to 2 (bias is high -0.71 for GOES-16 and 1.25 for Meteosat-10 and high SD). Pixels with QL equal to 2 should be used use with precaution.

*Table 4: GOES-16. Statistics of the difference between satellite SST and drifting buoy measurements presented per quality level (QL). Mean (Bias), standard deviation (SD). N is the number of match-ups.*

| | Night | | | Day | | |
|---|---|---|---|---|---|---|
| QL | N | Bias | SD | N | Bias | SD |
| 5 | 112679 | 0.09 | 0.36 | 93519 | 0.20 | 0.35 |
| 4 | 85307 | -0.02 | 0.41 | 84373 | 0.14 | 0.37 |
| 3 | 59995 | -0.19 | 0.48 | 70798 | 0.04 | 0.43 |
| 2 | 265709 | -0.71 | 1.89 | 273062 | -0.40 | 1.71 |

*Table 5: Meteosat-10. Statistics of the difference between satellite SST and drifting buoy measurements presented per quality level (QL). Mean (Bias), standard deviation (SD). N is the number of match-ups.*

| | Night | | | Day | | |
|---|---|---|---|---|---|---|
| QL | N | Bias | SD | N | Bias | SD |
| 5 | 39858 | -0.09 | 0.41 | 67794 | -0.05 | 0.42 |
| 4 | 35237 | -0.17 | 0.52 | 54761 | -0.13 | 0.56 |
| 3 | 25077 | -0.34 | 0.58 | 38223 | -0.29 | 0.61 |
| 2 | 68001 | 1.25 | -0.53 | 102001 | -0.68 | 1.39 |

*Table 6: Meteosat-9. Statistics of the difference between satellite SST and drifting buoy measurements presented per quality level (QL). Mean (Bias), standard deviation (SD). N is the number of match-ups.*

| | Night | | | Day | | |
|---|---|---|---|---|---|---|
| QL | N | Bias | SD | N | Bias | SD |
| 5 | 7887 | -0.03 | 0.38 | 12629 | 0.05 | 0.38 |
| 4 | 8919 | -0.01 | 0.56 | 19608 | 0.11 | 0.59 |
| 3 | 8937 | -0.01 | 0.67 | 7905 | -0.05 | 0.69 |
| 2 | 25036 | -0.05 | 1.66 | 33790 | 0.08 | 1.77 |

Time series of daily statistics are presented on figures 2, 3 and 4 for quality level 3, 4 and 5 together and for day and night time separately. One can observe missing data in the time series at the beginning of 2022 year for GOES-16.

Overall the statistics are stable over the period considered. No major difference is apparent in the stability during night-time and day-time. Meteosat-9 standard deviation (and robust standard deviation) displays slightly more variability over time than the other satellites.

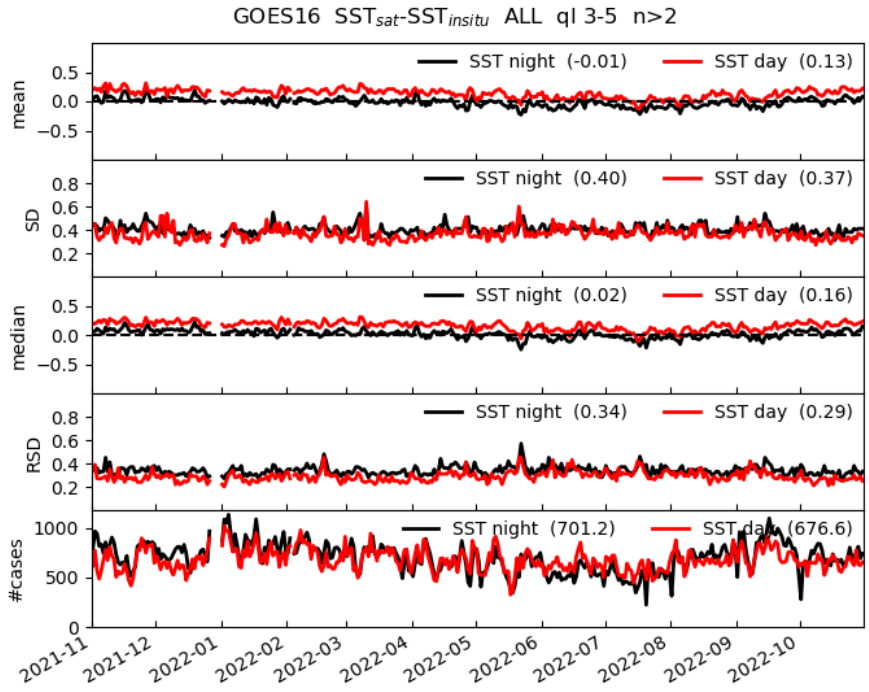


*Figure 2: GOES-16. Time evolution of the daily mean bias, standard deviation, median, robust standard deviation and number of match-ups (from top to bottom) for the comparison to drifting buoy measurements.*

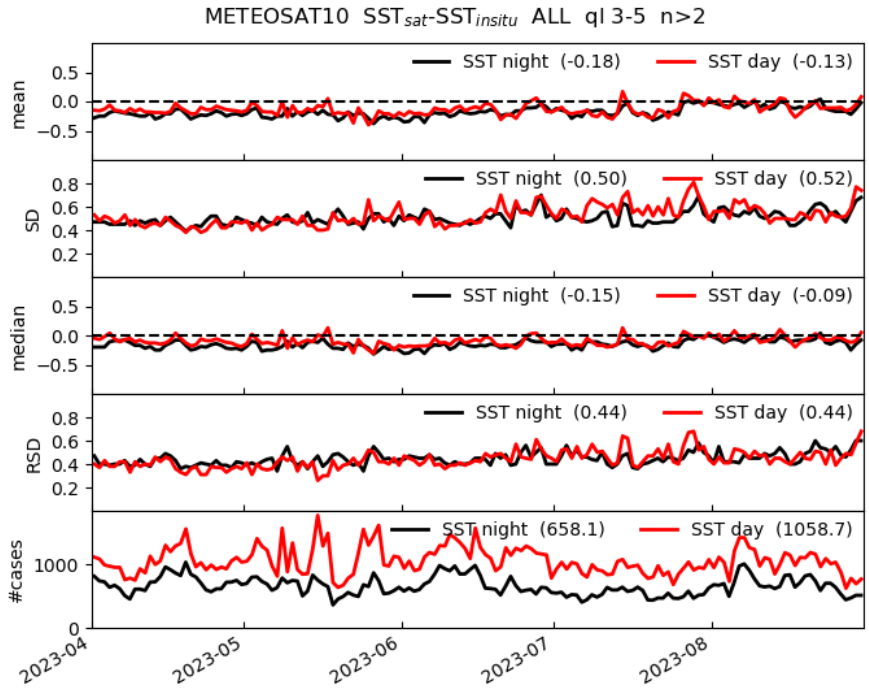


*Figure 3: Meteosat-10. Time evolution of the daily mean bias, standard deviation, median, robust standard deviation and number of match-ups (from top to bottom) for the comparison to drifting buoy measurements.*

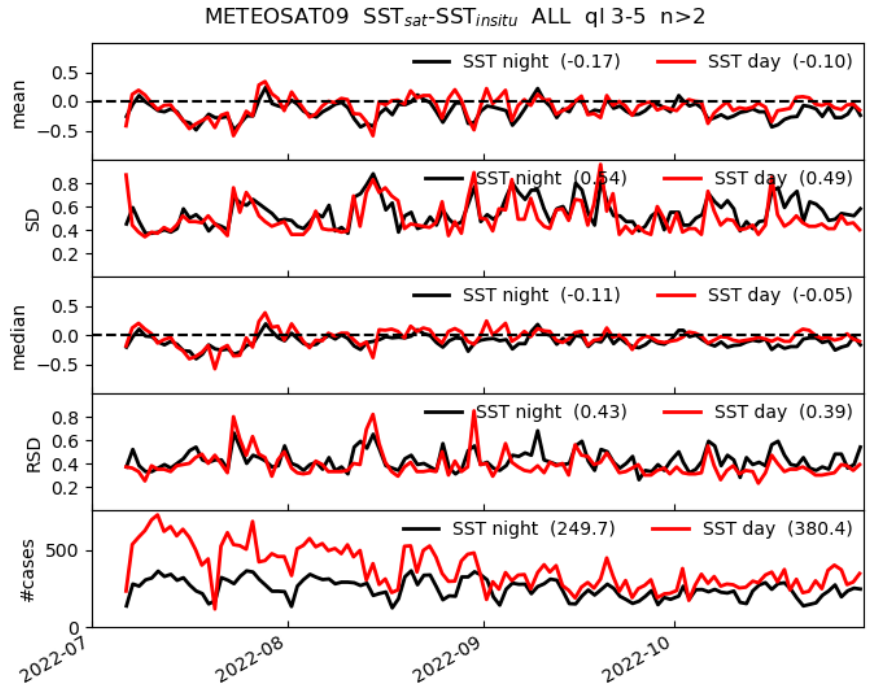


*Figure 4: Meteosat-9. Time evolution of the daily mean bias, standard deviation, median, robust standard deviation and number of match-ups (from top to bottom) for the comparison to drifting buoy measurements.*

*Table 7: Statistics of the difference between satellite SST and drifting buoy measurements computed monthly for each satellite: Mean (Bias), standard deviation (SD). N is the number of match-ups.*

| | | Night | | | Day | | |
|---|---|---|---|---|---|---|---|
| satellite | month | N | mean | SD | N | mean | SD |
| GOES-16 | 2021-11 | 22989 | 0.06 | 0.43 | 19831 | 0.20 | 0.37 |
| GOES-16 | 2021-12 | 19901 | 0.04 | 0.38 | 17607 | 0.19 | 0.36 |
| GOES-16 | 2022-01 | 26405 | 0.00 | 0.39 | 23697 | 0.16 | 0.37 |
| GOES-16 | 2022-02 | 22283 | 0.01 | 0.40 | 20975 | 0.18 | 0.37 |
| GOES-16 | 2022-03 | 22373 | -0.01 | 0.39 | 22063 | 0.18 | 0.32 |
| GOES-16 | 2022-04 | 19696 | -0.02 | 0.41 | 20236 | 0.15 | 0.37 |
| GOES-16 | 2022-05 | 19152 | -0.06 | 0.41 | 19826 | 0.10 | 0.38 |
| GOES-16 | 2022-06 | 16267 | -0.07 | 0.41 | 18953 | 0.07 | 0.40 |
| GOES-16 | 2022-07 | 15846 | -0.10 | 0.40 | 18037 | 0.01 | 0.39 |
| GOES-16 | 2022-08 | 22112 | -0.06 | 0.40 | 21155 | 0.06 | 0.38 |
| GOES-16 | 2022-09 | 24937 | -0.04 | 0.43 | 22069 | 0.11 | 0.40 |
| GOES-16 | 2022-10 | 21582 | 0.03 | 0.39 | 20071 | 0.18 | 0.33 |
| Meteosat-10 | 2023-04 | 21475 | -0.22 | 0.47 | 31112 | -0.15 | 0.46 |
| Meteosat-10 | 2023-05 | 20048 | -0.23 | 0.48 | 35043 | -0.16 | 0.49 |
| Meteosat-10 | 2023-06 | 21414 | -0.20 | 0.51 | 34973 | -0.14 | 0.53 |
| Meteosat-10 | 2023-07 | 16423 | -0.16 | 0.53 | 28732 | -0.13 | 0.62 |
| Meteosat-10 | 2023-08 | 21183 | -0.08 | 0.54 | 31715 | -0.07 | 0.56 |
| Meteosat-9 | 2022-07 | 8074 | -0.18 | 0.52 | 14973 | -0.14 | 0.56 |
| Meteosat-9 | 2022-08 | 8493 | -0.16 | 0.57 | 13349 | -0.08 | 0.55 |
| Meteosat-9 | 2022-09 | 6707 | -0.12 | 0.60 | 8592 | -0.05 | 0.56 |
| Meteosat-9 | 2022-10 | 6961 | -0.20 | 0.57 | 9256 | -0.10 | 0.49 |

Table 7 shows the monthly statistics for each satellite for twelve month for GOES-16 and Meteosat-10 and for four month for Meteosat-9. The values of mean and standard deviation of the temperature difference between satellite and drifting buoy measurements are well within the target accuracy defined in [AD.1].

### 3.3 Regional statistics

In this section results of the comparisons to drifting buoys are presented regionally. Monthly maps of the median of the difference to drifting buoys measurements are presented on Figure 5. The median stay small across the domains with values very occasionally reaching close to 1K. It is to be noted that large biases are quite consistently associated with a low number of collocations (see figure 7) and a high robust standard deviation (see figure 6). In particular one can notice the very low number of data points in the Southern Seas also corresponding to high satellite zenith angle.

One can notice a negative bias in the Northern hemisphere (particularly visible during night-time for GOES-16) and a positive bias in the Southern hemisphere. Further investigations (not shown here) have shown the seasonality of this observation: it is more pronounced during late spring and summer months. While these biases are not large, they remain unexplained. Similar feature is also apparent on Metop/AVHRR validation results.

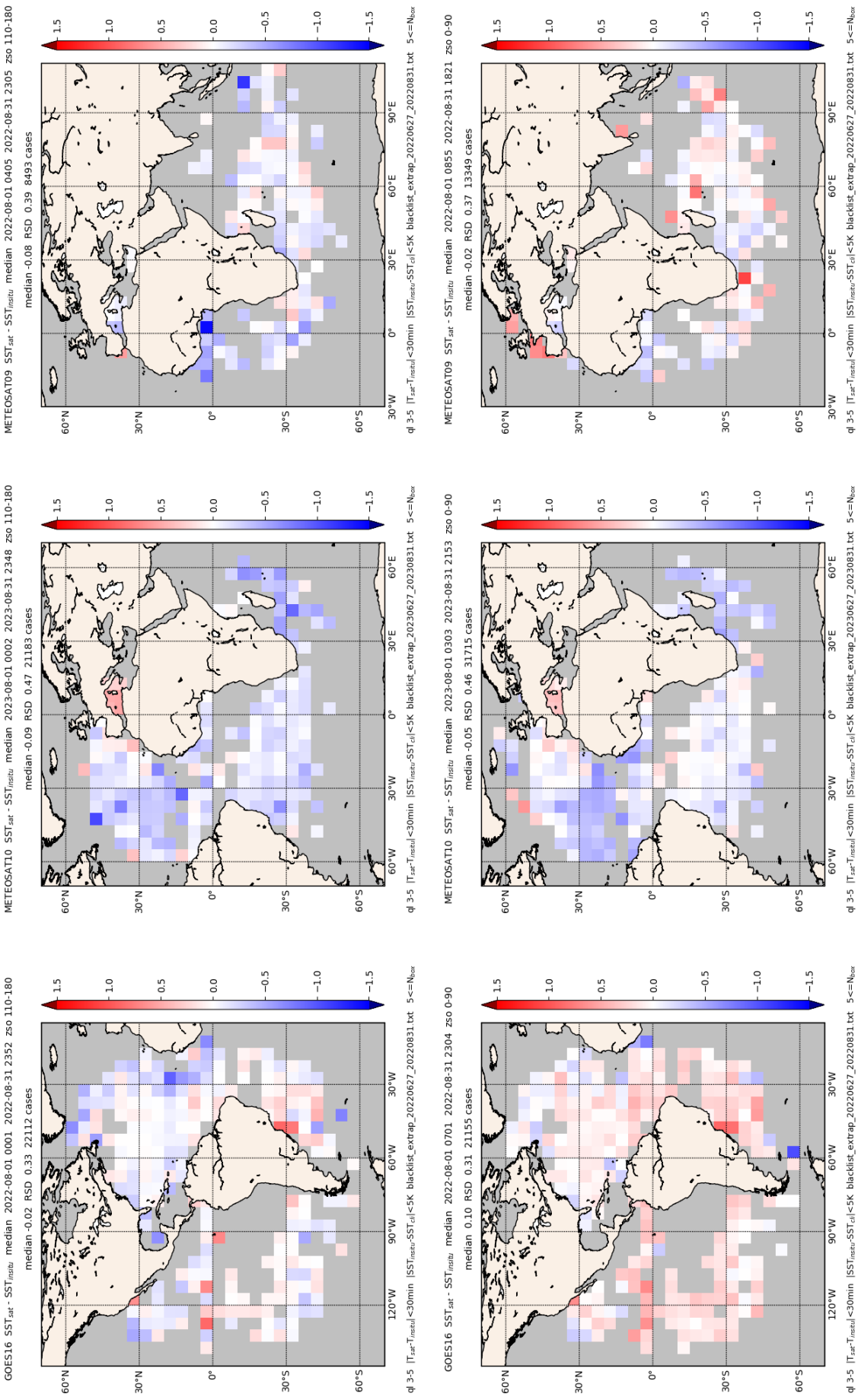


*Figure 5: Monthly median (August 2022 for GOES-16 and Meteosat-9 ; August 2023 for Meteosat-10) of the difference [satellite SST minus drifting buoys SST] for night-time (top) and day-time (bottom): GOES-16 (left), Meteosat-10 (left), and Meteosat-9 (right).*

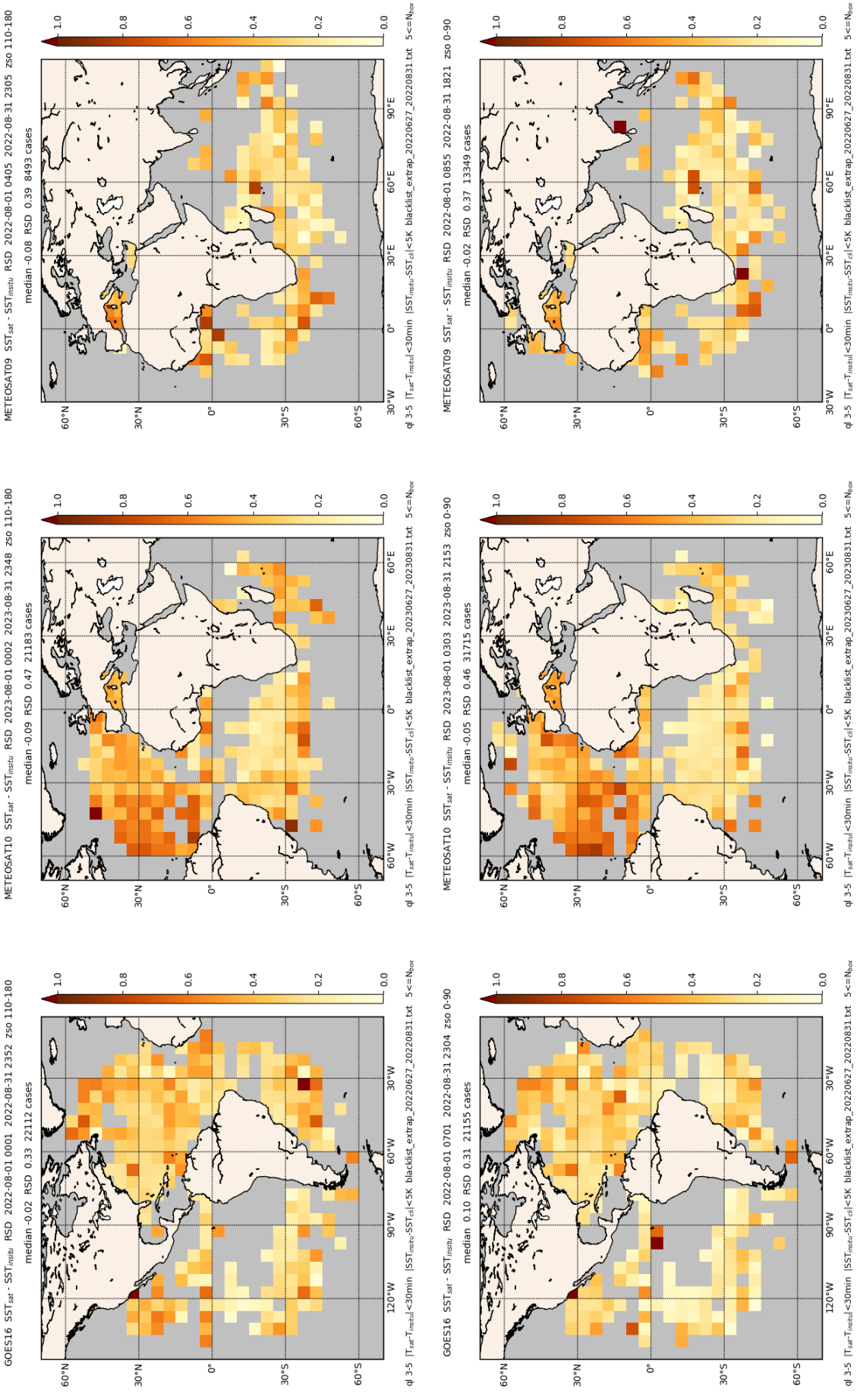

*Figure 6: Monthly robust standard deviation (August 2022 for GOES-16 and Meteosat-9 ; August 2023 for Meteosat-10) of the difference [satellite SST minus drifting buoys SST] for night-time (top) and day-time (bottom): GOES-16 (left), Meteosat-10 (left), and Meteosat-9 (right).*

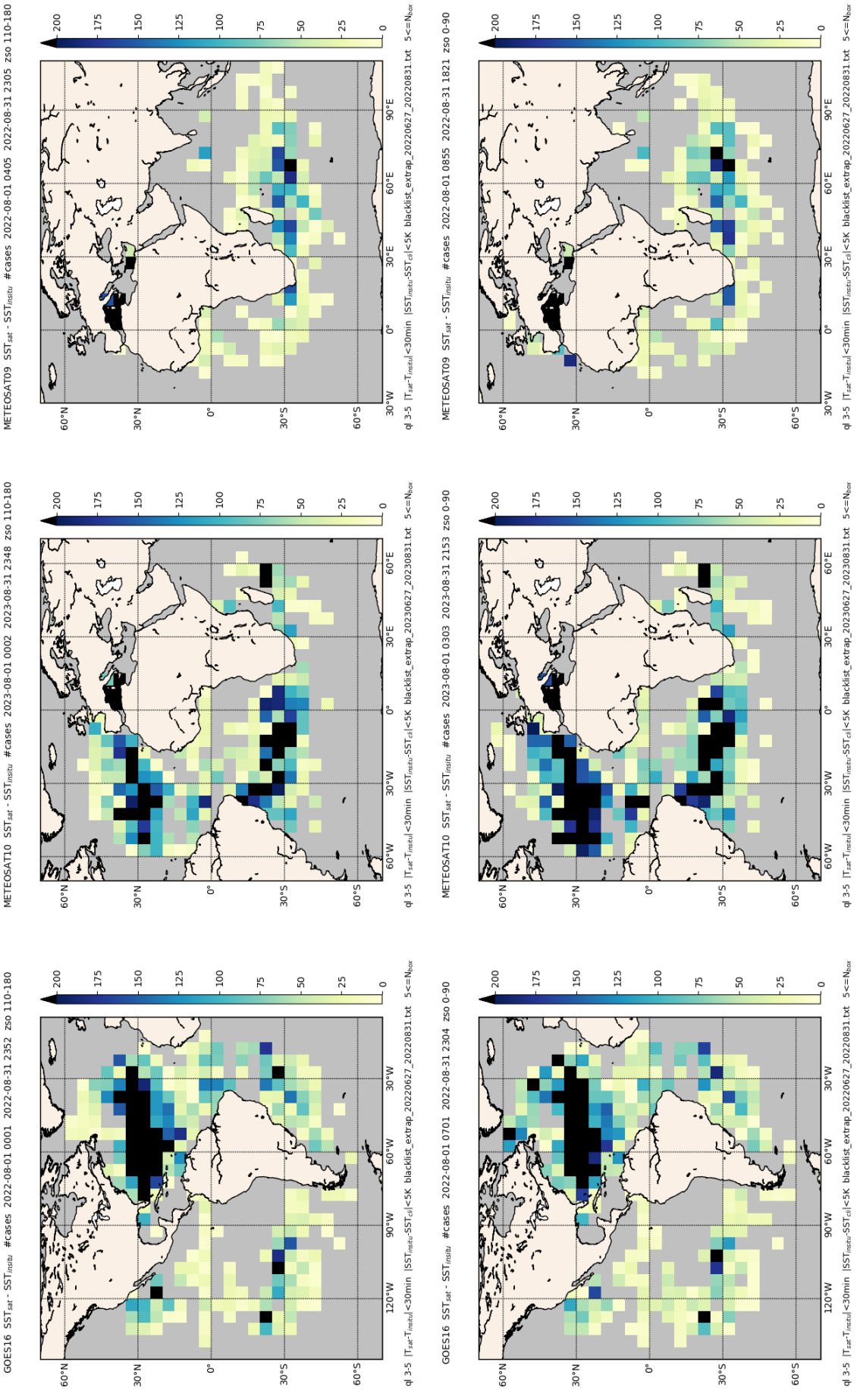


*Figure 7: Monthly number of match-ups (August 2022 for GOES-16 and Meteosat-9 ; August 2023 for Meteosat-10) between satellite SST and drifting buoys SST for night-time (top) and day-time (bottom): (left), Meteosat-10 (left), and Meteosat-9 (right).*

### 3.4 SST dependencies

Another informative way of looking at the comparison with in situ data is to plot the difference satellite SST minus in situ SST as a function of some other variables. Figures 8, 9 and 10 display such plots with respect to in situ SST, satellite zenith angle, latitude and longitude for GOES-16, Meteosat-10 and Meteosat-9 respectively.

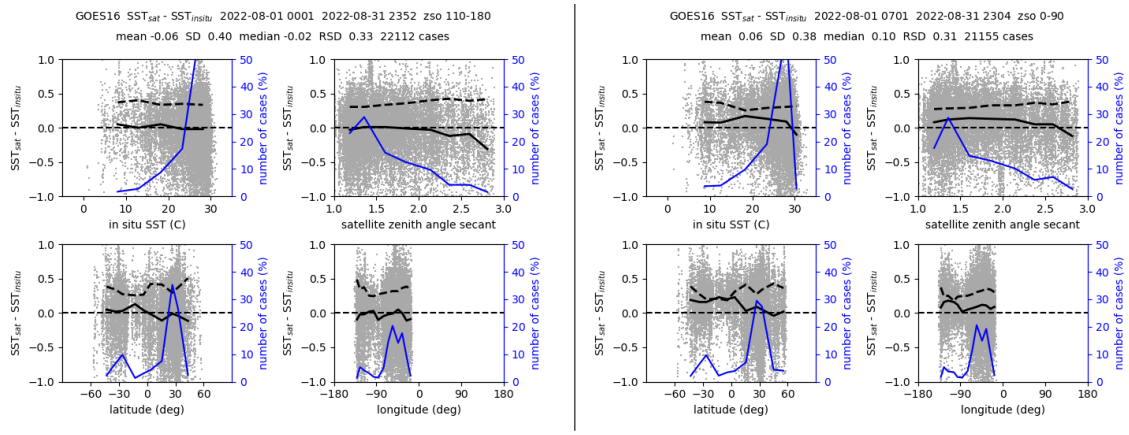


*Figure 8: August 2022. Bias (black line) and standard deviation (black dashed line) of the difference GOES-16 SST minus drifting buoy SST plotted as a function of in situ SST, satellite zenith angle, longitude and latitude: night -time on the left and day-time on the right.*

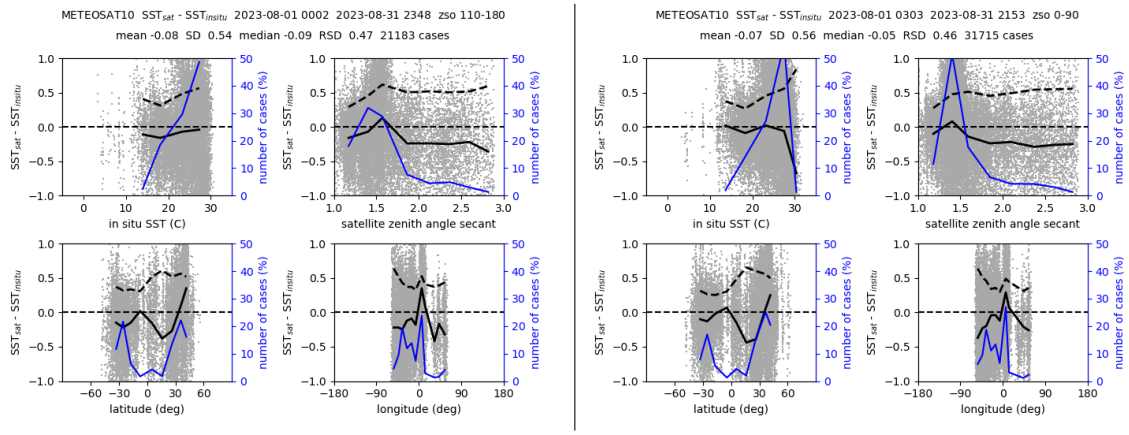


*Figure 9: August 2023. Bias (black line) and standard deviation (black dashed line) of the difference Meteosat-10 SST minus drifting buoy SST plotted as a function of in situ SST, satellite zenith angle, longitude and latitude: night -time on the left and day-time on the right.*

On figure 8 for GOES-16 there is little variation in the SST difference with respect to in-situ SST, but a positive biais during day time is apparent. Also, as previously noted, the difference between North and South is quite visible on the latitude dependence plot.

On figure for Meteosat-10 (figure 9) there is a little negative variation with in situ SST on night but a variation a little bit more important with the satellite zenith angle. For Meteosat-9 an Meteosat-10 there is little variation with in-situ SST and satellite zenith angle. The longitude and latitude dependencies are very different between the two Meteosat satellites due to their respective field of view. On Meteosat-10 plots (figure 9), one can notice an increase of the bias around 35 degree of latitude and around 0 degree of longitude (during day and night-time). This is the signature of the Mediterranean Sea which display a significant positive bias, as seen in section 3.3. For Meteosat-9

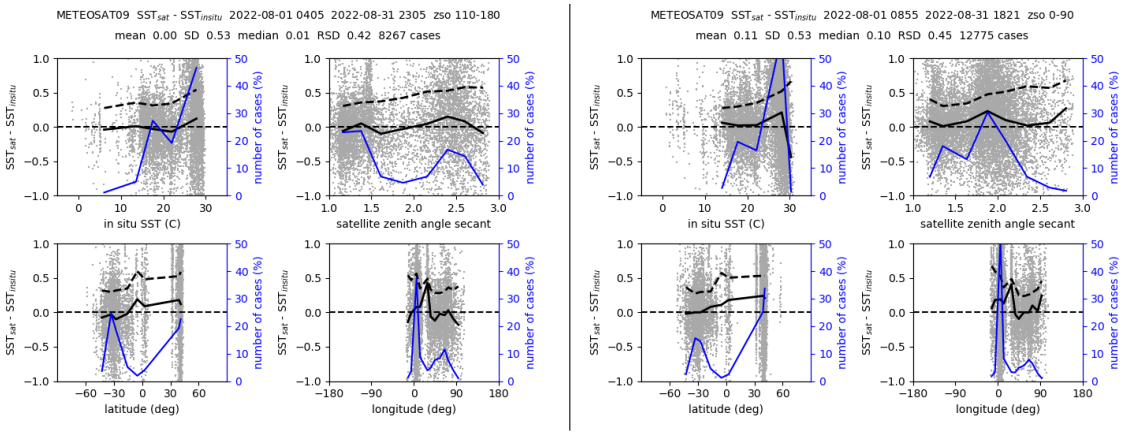


*Figure 10: August 2022. Bias (black line) and standard deviation (black dashed line) of the difference Meteosat-9 SST minus drifting buoy SST plotted as a function of in situ SST, satellite zenith angle, longitude and latitude: night -time on the left and day-time on the right.*

(figure 10) these are much less visible owing to a different algorithm (although using the same form and channels) and field of view.

Despite the above mentioned minor features, these plots do not show any strong anomalies.

# 4 Conclusion

The quality assessment of OSI SAF geostationary SST products (GOES-16, Meteosat-9 and Meteosat-10) shows coherent and stable results over time within the OSI SAF CDOP-4 requirements.

For Meteosat products, the comparison to drifting buoys is consistent with the state of the art and in particular with Merchant et al. (2009); Le Borgne et al. (2011).

GOES-16 product are noticeably better (in term of standard deviation) than Meteosat products. GOES-16 carries a new generation instrument, the Advanced Baseline Imager (ABI), which has more channel suitable for SST retrieval than Meteosat/Spinning Enhanced Visible and Infra Red Imager (SEVIRI). The algorithm designed for GOES-16/ABI make use of three channels (8.5, 10.3 and 12.3$\mu$m) making it more robust to varying atmospheric conditions (water vapour in particular).

## References

Donlon, C. J., Martin, M., Stark, J., Roberts-Jones, J., Fiedler, E., and Wimmer, W. (2012). The operational sea surface temperature and sea ice analysis (OSTIA) system. *Remote Sensing of Environment*, 116:140—-158.

Le Borgne, P., Roquet, H., and Merchant, C. (2011). Estimation of sea surface temperature from the spinning enhanced visible and infrared imager, improved using numerical weather prediction. *Remote Sensing of Environment*, 115(1):55–65.

Marsouin, A., Le Borgne, P., Legendre, G., Péré, S., and Roquet, H. (2015). Six years of OSI-SAF METOP-A AVHRR sea surface temperature. *Remote Sensing of Environment*, 159:288–306.

McCain, E. P., Pichel, W. G., and Walton, C. C. (1985). Comparative performance of AVHRR-based multichannel sea surface temperature. *Journal of Geophysical Research*, 90:11587–11601.

Merchant, C. J., Le Borgne, P., Roquet, H., and Marsouin, A. (2009). Sea surface temperature from a geostationary satellite by optimal estimation. *Remote Sensing of Environment*, 113(2):445–457.

Walton, C. C., Pichel, W. G., Sapper, J. F., and May, D. A. (1998). The development and operational application of nonlinear algorithms for the measurement of sea surface temperatures with the NOAA polar-orbiting environmental satellites. *Journal of Geophysical Research*, 103:27999–28012.